NEOPLASMA accepted, ahead of print manuscript
Cite article as https://doi.org/10.4149/neo_2025_250110N12

Running title: WTAP inhibits melanoma progression

WTAP is a promising diagnosis and treatment biomarker that inhibits the proliferation and invasion of melanoma cells

Huixiu Lu[1,2,#], Yanli Zhang[1,#], Jiali Li[3,4], Dan Lou[5], Licui Li[6], Yunchuan Liang[2], Jianying Li[2], Yaling Liu[1,*]

[1]Department of Dermatology and Venereology, The Third Hospital of Hebei Medical University, Shijiazhuang, Hebei, China; [2]Department of Dermatology, Shijiazhuang People's Hospital, Shijiazhuang, Hebei, China; [3]Research Center, The Fourth Hospital of Hebei Medical University, Shijiazhuang, Hebei, China; [4]Key Laboratory of Tumor Prevention, Precision Diagnosis and Treatment of Hebei, Clinical Oncology Research Center, The Fourth Hospital of Hebei Medical University, Shijiazhuang, Hebei, China; [5]Department of Pathology, Shijiazhuang People's Hospital, Shijiazhuang, Hebei, China; [6]Department of Dermatology, Shijiazhuang Gaocheng People's Hospital, Shijiazhuang, Hebei, China

*Correspondence: yzling_liu2023@hebmu.edu.cn

[#]Contributed equally to this work.

Received January 10, 2025 / Accepted May 13, 2025

Wilms' tumor 1-associating protein (WTAP) is ubiquitously expressed in many tissues and plays an important role in physiological processes and tumor development. Here, we investigated the specific biological role and underlying mechanism of WTAP in melanoma. We determined the expression of WTAP and its correlation with clinicopathological features in paraffin-embedded tissues. We investigated the effects of WTAP on melanoma cells via a CCK-8 assay, a colony formation assay, an EdU assay, a Transwell assay, and subcutaneous xenograft experiments. We then applied RNA sequencing to further screen candidate targets, and NT5E was selected as the downstream gene of WTAP. Finally, a series of rescue assays, together with nucleotidase assays and ELISA, were adopted to confirm the function of NT5E in melanoma progression. We demonstrated that WTAP expression was downregulated in melanoma, which was associated with a poor prognosis, and that WTAP expression served as an independent predictor of melanoma survival. Functionally, WTAP hindered the proliferation, growth, migration, and invasion of melanoma cells. Furthermore, NT5E was identified as the downstream effector of WTAP and was subsequently found to rescue the increased proliferation, migration, and invasion of melanoma cells induced by WTAP deficiency. Moreover, knockdown of WTAP increased the expression of NT5E, MMP2, and N-cadherin, and simultaneous transfection with siNT5E reversed the increased expression of MMP2 and N-cadherin. Moreover, increased NT5E expression caused by forced WTAP inhibition in melanoma promoted the hydrolysis of AMP to produce more adenosine and further abrogated the secretion of IFN-γ by PBMCs. We found that WTAP expression is significantly downregulated and

restrains the progression of melanoma via the downstream effects of NT5E on immunosuppression and molecular adhesion. This study revealed that WTAP plays a crucial inhibitory role in melanoma oncogenesis and highlighted WTAP as a potential novel diagnosis and therapeutic target for melanoma.

Key words: Wilms′ tumor 1-associated protein (WTAP); melanoma; ecto-5′-nucleotidase (NT5E); immunosuppression; adhesive molecule

Melanoma is one of the most aggressive human cancers, which originates from melanocytes, namely, melanin producing cells that are located mainly in the skin, but are also found in the mucosa, uvea, and leptomeninges. The incidence of melanoma has rapidly increased over the course of the last few decades, far exceeding that of other types of malignant tumor [1]. Melanoma is characterized by a tendency to metastasize, and patients with metastatic disease have a worse prognosis [2]. The 5-year relative survival rate of patients with localized or regional melanoma has been shown to be 98% and 64%, respectively, whereas in patients with metastatic melanoma, the 5-year survival rate is only 20% [3]. Cutaneous melanoma, which is driven by exposure to ultraviolet radiation from sunshine or tanning beds [4, 5], is responsible for the majority of melanoma cases, accounting for > 75% of skin cancer associated deaths [3]. Over the last few decades, great progress has been made in terms of elucidating the underlying mechanisms of cutaneous melanoma at the molecular, cellular, and organismal levels; however, the 5-year survival rate remains unsatisfactorily low. Therefore, a more in-depth understanding of the mechanism of melanoma development is urgently required to facilitate the development of novel therapies that may be used to target this potentially fatal disease.

N6-methyladenosine (m6A) modification, the most prevalent internal modification of mRNAs [6, 7], has been reported to fulfil several roles in the regulation of gene expression in eukaryotes, including its participation in RNA stability, splicing and translation efficacy [8]. This dynamic and reversible modification is catalyzed by the m6A methyltransferase complex, in which Wilms' tumor 1-associated protein (WTAP) serves as a key regulatory subunit to stabilize the core catalytic components methyltransferases methyltransferase-like 3 (METTL3) and methyltransferase-like 14 (METTL14), ensuring their proper localization to nuclear speckles and efficient m6A deposition on target RNAs [9, 10]. As a key component of m6A, WTAP has been shown to be essential in many cellular processes, including alternative splicing, X chromosome inactivation and cell cycle

regulation [11-13]. Moreover, dysregulation of WTAP has been shown to be linked to multiple cancers, where it often acts as an oncogenic driver, contributes to the aggressive features of various types of cancers, including hepatocellular carcinoma, osteosarcoma, ovarian cancer and colorectal cancer [14-17]. Meanwhile, the tumor suppressor role of WTAP has been reported in several bioinformatics studies [18-20]. However, the biological role of WTAP in melanoma, one of the most aggressive malignancies, has yet to be fully elucidated. Feng et al. [21] downloaded the RNA sequencing transcriptomic data and clinical information of patients with melanoma from the Genotype Tissue Expression and The Cancer Genome Atlas databases, and identified that WTAP is an independent protective prognostic factor for melanoma patients. Finally, the function of WTAP in melanoma cells was verified via plasmid transfection into A375 cells. In spite of these advances in our knowledge, however, how WTAP affects melanoma progression has yet to be fully elucidated.

Ecto-5′-nucleotidase (NT5E; also known as CD73) is a 70 kDa glycosylphosphatidylinositol-anchored cell surface protein that is widely distributed in the outer leaflet of the plasma membrane. As a nucleotidase, NT5E catalyzes the hydrolysis of adenosine monophosphate (AMP) into adenosine and phosphate. A high level of NT5E gene expression in tumor cells has been shown to be conducive to the accumulation of the immunosuppressive molecule adenosine in the tumor microenvironment, thereby promoting tumor growth and metastasis [22]. In addition, NT5E-generated adenosine was able to mediate the immune evasion of tumor cells via attenuating the functions of multiple types of immune cells, resulting in immune escape and further tumor growth and metastasis [23]. In addition to its effects on adenosine, NT5E has also been shown to function as an adhesive molecule that regulates cellular interactions with components of extracellular matrix (ECM) to mediate cancer cell adhesion and migration, as well as stemness [24-26]. There is increasing evidence to show that NT5E is overexpressed in numerous types of cancer, and that this high expression is positively associated with tumor malignancy and poor outcomes [27-29]. In light of its multiple effects on tumor progression as a potential checkpoint, anti-NT5E therapy has recently attracted attention as an emerging area for therapeutic intervention in terms of cancer immunotherapy, especially in combination with conventional therapy and/or treatment with other immune checkpoint inhibitors [30-32]. An in-depth study demonstrated that an absence of NT5E improved survival in a murine model of glioblastoma treated

with anti-CTLA-4 and anti-PD-1 antibodies, and these researchers further concluded that NT5E acts as a specific immunotherapeutic target that is capable of improving anti-tumor immune responses to immune checkpoint therapies in glioblastoma [32]. A previous study also reported that NT5E blockade may limit both the production and activation of immunosuppressive adenosine molecules within the tumor microenvironment, thereby overcoming the development of immune resistance [33]. Furthermore, as previously reported, NT5E expression was shown to be correlated with the plasticity of melanoma cells, thereby expediting the transition from a proliferative to an aggressive phenotype [34]. In view of these findings, the present study aimed to provide novel insights into the molecular pathogenesis of melanoma, and the results obtained suggest that targeting WTAP via the potential downstream effects of NT5E on immunosuppression and adhesion holds promise as a novel means of therapeutic intervention.

Patients and methods

Public datasets. The Gene Expression Profiling Interactive Analysis (GEPIA) database (https://gepia.cancer-pku.cn/) was utilized to compare WTAP expression levels across various cancer types and their corresponding normal tissues, as well as to evaluate the correlation between WTAP expression and prognostic outcomes in melanoma patients.

Clinical samples and ethics. Paraffin-embedded tissue samples from 55 patients with melanoma who underwent surgical excision between January 2009 and December 2018 were obtained from the Department of Pathology of Shijiazhuang People's Hospital. Complete clinicopathological data, including follow-up information for all 55 patients, were collected from the medical records room of Shijiazhuang People's Hospital. The duration of follow-up was between January 2019 and March 2024. The inclusion criteria were as follows: i) a confirmed pathological diagnosis of melanoma; and ii) no prior therapy was received by the patient before surgery. The exclusion criteria were as follows: i) a previous history of malignant tumor; and ii) a previous history of immune system disease. The paraffin-embedded samples were used for subsequent immunohistochemistry analysis, as detailed below, to confirm the association between the expression of WTAP and the prognosis of patients with melanoma. All patients involved in the present study signed written informed consent statements prior to the surgery, and this study was approved by the Ethics Committee of Shijiazhuang People's Hospital (Approval No. 2024101).

139 **Immunohistochemistry (IHC).** According to the manufacturer's protocol, IHC staining was
140 conducted via the UltraSensitive TMSP (Mouse/Rabbit) IHC Kit (#PV-9000, ZSGB-Bio, China)
141 with the following primary antibodies: anti-WTAP antibody (1:1000, #60188-1-Ig, Proteintech,
142 China), anti-NT5E antibody (1:500, #12231-1-AP, Proteintech, China), anti-MMP2 antibody (1:200,
143 #10373-2-AP, Proteintech, China) and anti-N-cadherin antibody (1:4000, #22018-1-AP, Proteintech,
144 China). Briefly, the 4 μm, paraffin-embedded slides were deparaffinized with xylene followed by
145 rehydration with a decreasing alcohol gradient and PBS washing for three times. The sections were
146 then immersed with endogenous peroxidase blocker for 20 min at room temperature to suppress
147 endogenous peroxidase activity, and after three times washing by PBS, the tissue sections were
148 transferred into Citrate Antigen Retrieval Solution (#C1032, Solarbio, China) and heated in a
149 pressure cooker at high pressure for 2 min for antigen retrieval. Thereafter, the slides were
150 incubated with diluted antibodies at 4 °C overnight. Next, the slides were in turn incubated with
151 reaction strengthening fluid and enhanced enzyme-labeled goat anti-Mouse/Rabbit IgG polymer at
152 37 °C for 20 min, respectively. Finally, color development was carried out with DAB (#ZLI-9018,
153 ZSGB-Bio, China) for 5 min at room temperature and then slides were counterstained with Harris
154 hematoxylin (#BA4097, Baso, China), and dehydrated using a series of increasing alcohol
155 concentrations, and cover slipped. The WTAP staining score for each patient was computed by
156 multiplying the staining intensity grade (a grade of 0, 1, 2 or 3 indicated negative, weakly positive,
157 moderately positive or strongly positive staining, respectively) and positive percentage score (a
158 score of 0, 1, 2, or 3 indicated a positive percentage of 0-25%, 26-50%, 51-75% or 76-100%,
159 respectively).
160 **Cell lines and cell culture.** Human melanoma cell lines A875 (TCH C203) and A375 (TCH C114)
161 were provided by Suzhou Haixing Biosciences Co., Ltd. Both cell lines were authenticated by short
162 tandem repeat profiling analysis, and mycoplasma contamination was ruled out using the MycoEasy
163 Rapid Mycoplasma Test Kit (#CA6101024, Cellapy, China). Routinely, the cells were cultured in
164 Gibco® Dulbecco's modified Eagle's medium (DMEM, Gibco, USA) supplemented with 10% fetal
165 bovine serum (FBS, Gibco, USA) and 1% penicillin/streptomycin (Invitrogen, USA) in a 5% CO_2
166 humidified atmosphere at 37 °C.
167 **RNA interference.** Small interfering RNAs (siRNAs) directed against WTAP (termed siWTAP)
168 and NT5E (termed siNT5E) and negative control RNAs (termed siNC) were synthesized by

169 RiboBio (Guangzhou, China). Transient transfection was performed with Invitrogen™
170 Lipofectamine® 2000 Reagent (Invitrogen, USA) according to the standard protocol. Cells
171 transfected with siWTAP or siNT5E were harvested 48 h post-transfection for RT-qPCR and
172 immunoblotting analyses or functional assays. For rescue experiments, siWTAP was transfected
173 first (for 24 h), followed by siNT5E transfection (for an additional 24 h). The sequences of the
174 siRNAs used were as follows: siWTAP-1: 5' -GGAACAGACTAAAGACAAA-3' ; siWTAP-2:
175 5' -CTAAGAGAGTCTGAAGAAA-3' ; siWTAP-3: 5' -GAAGCATATGTACAAGCTT-3' ;
176 siNT5E-1: 5' -GGAGATGGGTTCCAGATGA-3' ; siNT5E-2:
177 5' -GATCGAGTTTGATGAAAGA-3' ; siNT5E-3: 5' -GATGGCTCCTCTCAATCAT-3' .
178 **Plasmid transfection.** The WTAP-overexpressing plasmid (RC209632, termed oeWTAP) and
179 empty vector (#PS100001, termed oeVector) were constructed by OriGene Technologies, Inc.
180 Plasmid transfection in A875 and A375 cells was performed using jetPRIME® Versatile
181 DNA/siRNA transfection reagent (Polyplus-transfection SA), and 48 h later, the transfection
182 efficiency was evaluated. Cells that had been successfully transfected were harvested for
183 subsequent functional experiments. No selection markers were used in the present study.
184 **RNA isolation and quantitative real-time PCR (RT-qPCR).** Total RNA was isolated from A875
185 and A375 cells using TRIzol Reagent (Invitrogen, USA), followed by RNA concentration and
186 quality assessment using a NanoDrop One spectrophotometer (Applied Biosystems, USA). Total
187 RNA (2 μg) was reverse transcribed into cDNA using GoScript™ Reverse Transcription Mix
188 (Promega, USA) according to the manufacturer's instructions. For mRNA expression analysis, the
189 cDNA was amplified using GoTaq® qPCR Master Mix (Promega, USA) with an Applied
190 Biosystems™ StepOne Plus Real-Time PCR system (Applied Biosystems, USA). Relative
191 expression levels were normalized against those of GAPDH and calculated using the $2^{-\Delta\Delta cq}$ method
192 [35]. All the RT-qPCR reactions were performed in triplicate technical replicates for each biological
193 replicate to ensure data reliability and reproducibility, and the details of all primers used (including
194 their sequences) are shown in Table 1.
195 **Protein isolation and western blot.** A875 and A375 cells were seeded in 6-well plates and
196 routinely maintained in complete DMEM medium in a 5% CO_2 humidified atmosphere at 37 °C.
197 After achieving full cell adhesion and desired confluency, cells were transfected with either siRNA
198 or plasmids, with detailed methodologies provided in "RNA interference" and "Plasmid transfection"

above. 48 h later, total cellular proteins were extracted via precooled RIPA buffer (Sevenbio, China) containing protease inhibitors (Sevenbio, China), and a BCA protein assay kit (Sevenbio, China) was used to evaluate the protein concentration. An Omni-Easy™ Protein Sample Loading Buffer (LT101S, EpiZyme, China) was adopted to mix with 1:4 (v/v) protein sample followed by incubation at 100 °C for 5 min. Then, 30 μg total cellular proteins were subjected to electrophoresis on an SDS-PAGE (10%, Biotides, China) and transferred to a PVDF membrane (Millipore, USA) followed by membrane incubation in rapid blocking buffer (#G2052-500ml, Servicebio, China) for 10 mins at room temperature to prevent non-specific binding. After incubation with primary anti-WTAP (1:10000, #60188-1-Ig, Proteintech, China), anti-NT5E (1:1000, #12231-1-AP, Proteintech, China), anti-MMP2 (1:800, #10373-2-AP, Proteintech, China), anti-N-cadherin (1:3000, #22018-1-AP, Proteintech, China) and anti-β-actin (1:2500, #20536-1-AP, Proteintech, China) antibodies at 4 °C overnight, the membranes were then incubated with HRP-conjugated Goat Anti-Mouse antibody (#SA00001-1, Proteintech, China) or HRP-conjugated Goat Anti-Rabbit antibody (#SA00001-2, Proteintech, China) at 37 °C for 1 h. Finally, the signals were detected via a ChemiDoc TM MP Imaging system (Bio-Rad Laboratories, Inc.) after the PVDF membrane has been immersed in SuperKine TM ECL reagent (#BMU102-CN2, Abbkine, China) for 2 min. All the western blot experiments were performed with triplicate independent biological replicates to ensure data reliability and reproducibility.

Cell proliferation assay. Cell proliferation ability was assessed with a Cell Counting Kit-8 (CCK-8, Kumamoto, Japan) based on the reduction of WST-8 (a water-soluble tetrazolium salt) to a water-soluble orange formazan via intracellular dehydrogenases in metabolically active cells. The absorbance at 450 nm is directly proportional to the number of viable cells. Pretreated cells were seeded into a 96-well plate at 2×10^3 cells/well with five replicates and cultured for 1, 2, 3, 4 or 5 days at 37 °C. At the same time, cell free blank wells were prepared to rule out the potential impact of background absorbance. Absorbance at 450 nm was detected by using the microplate reader (Tecan Group, Ltd.) daily to evaluate cell proliferation. To guarantee the robustness and repeatability of the experimental results, all CCK-8 assays were conducted using three independent biological replicates.

Colony formation assay. A total of 1.5×10^3 transfected A875 or A375 cells were inoculated into 6-well plates and incubated routinely in DMEM at 37 °C for 1-2 weeks until visible colonies

229 formed (colonies typically consist of > 50 cells). Colonies were fixed with 4% paraformaldehyde
230 (#P0099, Beyotime, China) at room temperature for 30 min and subsequently stained with 0.1%
231 crystal violet (#C0121, Beyotime, China) at room temperature for 15 min. Visible cell clusters were
232 captured under a light microscope (Olympus Corporation), and the numbers of cell colonies were
233 quantified using ImageJ software (version 1.8.0; National Institutes of Health). Each colony
234 formation experiment was carried out in triplicate with biologically independent samples for
235 enhanced data reliability and reproducibility.

236 **5-Ethynyl-2'-deoxyuridine (EdU) assay.** A VF 555 Click-iT EdU Universal Cell Proliferation
237 Detection Kit (#HY-K1086, MedChemExpress, USA) was performed to assess the cell proliferation
238 ability with triplicate independent biological replicates. According to the manufacturer's protocol,
239 transfected A875 or A375 cells were plated on glass coverslips in 12-well plates at a density of 3 ×
240 10^5 cells/well. After 24 h of routine inoculation, the cells were incubated with 50 μM EdU buffer at
241 37 °C for 2 h, fixed with 4% formaldehyde and permeabilized with 0.5% Triton X-100. Then, 500
242 μl Click-iT working buffer was added to each well, and the nuclei were stained with
243 4′,6-diamidino-2-phenylindole (DAPI) (#SI103-11, Sevenbio, China). Finally, images were
244 captured using a confocal microscope (LSM 900, Zeiss, Germany).

245 **Wound healing assay.** Pretreated A875 or A375 melanoma cells in the exponential growth phase
246 were seeded in a six-well plate. After 24 h incubation at 37 °C, when the cell confluence had
247 reached 90%, a 200 μl pipette tip was used to create two vertical bottom lines on the cells. The cells
248 were rinsed three times and then cultured in fresh serum-free medium. Images of the cell monolayer
249 were taken using an inverted microscope (Leica, Germany) at the 0 h and 48 h. The scratch wound
250 healing rate was assessed by measuring the migration distance using the following method: Cell
251 migration rate (%) = [(wound width at 0 h - wound width at 48 h) / wound width at 0 h] × 100%.
252 For enhanced data reliability and reproducibility, each wound healing experiment was carried out in
253 triplicate independent biological samples.

254 **Transwell migration and invasion assays.** Transwell assays were implemented in 24-well
255 Transwell™ plates (Corning Incorporated, USA) with an 8 μm pore size insert. For migration assay,
256 single-cell suspensions with 4 × 10^4 posttransfection cells were prepared with 100 μl of DMEM free
257 of FBS. These cells were seeded into the upper chamber, and the bottom chamber was filled with
258 600 μl of DMEM supplemented with 20% FBS. For invasion assay, the Transwell membranes were

pre-coated with 20 μl 1:7 diluted Matrigel (BD Biosciences, Franklin Lakes, NJ, USA) and allowed to solidify at 37 °C overnight. The subsequent steps followed the same protocol as the migration assay. After 48 h incubation at 37 °C, a wet cotton swab was used to wipe away the non-migrating cells on the upper surface of the membrane, whereas the invasive cells at the bottom were fixed with 4% paraformaldehyde and stained with 0.1% crystal violet. Images of the migrated cells were captured using an inverted microscope (Leica, Germany) in five random fields in each filter, and the numbers of cells were counted using ImageJ software (version 1.8.0). All migration and invasion assays were conducted using three independent biological replicates.

RNA-seq analysis. Total RNA was extracted from A875 cells following transfection with siWTAP-2 or siNC via TRIzol Reagent. Total RNA was quantified using a NanoDrop ND 2000 spectrophotometer, and RNA integrity was examined using an Agilent Bioanalyzer 2100 (Agilent Technologies, USA). Library construction and RNA-seq analysis were subsequently performed at Applied Protein Technology (Beijing, China) with an Illumina NovaSeq 6000 System (Illumina, USA), followed by computational analysis, which was also provided by this company.

Immunofluorescence assay. Pretreated cells were seeded on glass coverslips in 12-well plates at a density of 1×10^5 cells/well. After 24 h incubation at 37 °C, 4% paraformaldehyde and 0.3% Triton X-100 were added to each well for 15 and 5 min respectively to fix and permeabilize the cells, followed by blocking non-specific binding with 10% BSA. Anti-NT5E antibody (1:100, #12231-1-AP, Proteintech, China) was added to each well and incubated with the contents of the wells at 4 °C overnight, followed by incubation with goat anti-rabbit IgG (1:200, #SA00013-2, Proteintech, China) at room temperature for 1 h. After the cells had been stained with DAPI, images of the cells were captured using a confocal microscope (LSM 900, Zeiss, Germany).

Ectonucleotidase assay. To determine the enzymatic activity of NT5E hydrolysis, an ectonucleotidase assay was performed as previously described [36]. In brief, A875 or A375 cells pretreated with siWTAP were reseeded into 24-well plates at a density of 1.0×10^5 cells/well. After 24 h incubation at 37 °C, 200 μl reaction medium containing 2 mM $MgCl_2$, 120 mM NaCl, 5 mM KCl, 10 mM glucose, 20 mM HEPES and 2 mM AMP (#HY-A0181, MedChemExpress, USA) as the substrate was added to each reaction, and incubated at 37 °C for 45 min. Subsequently, 200 μl incubation medium was rapidly withdrawn and heat-inactivated at 95 °C for 90 sec to halt the enzymatic activity, and the mixture was subsequently centrifuged at 16,000 × g at 4 °C for 30 min.

289 The level of soluble free inorganic phosphate in each sample was detected with a Malachite Green
290 Phosphate Detection Kit (#S0196S, Beyotime, China) according to the manufacturer's instructions.
291 In addition, (a,b-methylene) diphosphate (APCP) (#HY-112502, MedChemExpress, USA) was
292 applied to investigate its effects on NT5E function, and 20 μM APCP was added to each sample 15
293 min prior to the addition of the substrate AMP. At the same time, the same volume of solvent was
294 added as a control.

295 **RNA immunoprecipitation (RIP).** To investigate WTAP-NT5E regulatory interactions, RIP
296 assays were performed in A875 and A375 cells transfected with either siWTAP or control siNC for
297 48 h using the Magna RIP™ Kit (Millipore, USA) following standardized protocols. Cells were
298 lysed in RIP lysis buffer for 15 min at 4 °C, followed by centrifugation at 12,000 × g for 10 min.
299 The resulting supernatant were collected and incubated with protein A/G magnetic beads
300 conjugated with anti-WTAP antibody (1:1000, #ab195380, USA) or anti-IgG antibody (1:5000,
301 #10284-1-AP, Proteintech, China) in RIP immunoprecipitation buffer (containing 0.5 M EDTA and
302 RNase inhibitor) overnight at 4 °C. Bead complexes were washed six times with ice-cold RIP wash
303 buffer, followed by proteinase K digestion (55 °C, 30 min) to release RNA. Recovered RNA was
304 purified using TRIzol Reagent and analyzed by RT-qPCR to quantify NT5E transcript enrichment
305 in WTAP pulldowns relative to IgG controls.

306 **Actinomycin D assay.** Following transfection with either siWTAP or negative control siNC, A875
307 and A375 cells were exposed to 2 μg/ml actinomycin D (Act D) for 0, 4, 8, 12 and 24 h to inhibit de
308 novo RNA transcription. Total RNA was isolated at the indicated time points and analyzed by
309 RT-qPCR. The expression levels of NT5E were normalized to GAPDH as an internal control, and
310 the relative half-life of NT5E was subsequently determined to assess its stability under WTAP
311 knockdown conditions.

312 **Enzyme-Linked Immunosorbent Assay (ELISA).** Peripheral blood mononuclear cells (PBMCs)
313 isolated from healthy donors via a human PBMC separation kit (#P5290, Solarbio, China) were
314 incubated in Gibco® RPMI-1640 medium (Gibco, USA) supplemented with 10% FBS and 1%
315 penicillin/streptomycin in a humidified atmosphere at 37 °C containing 5% CO_2. One day later, the
316 PBMCs (2×10^5 cells/well) were replated in 24-well plates, and incubated in 150 μl RPMI-1640
317 medium supplemented with FBS and penicillin/streptomycin and 50 μl supernatant from cultures of
318 melanoma cells or melanoma cells silenced with siNC, siWTAP or siNT5E. Phytohemagglutinin

319 (PHA) (10 μg/ml, #HY-N7038, MedChemExpress, USA) was added to stimulate the PBMCs to
320 produce interferon-γ (IFN-γ). In certain experiments, 2 mM AMP or 20 μM APCP was added to
321 each well. AZD4635 (50 nM, #HTL1071, MedChemExpress, USA), an A_{2A} adenosine receptor
322 antagonist, was added to each reaction to clarify the immunosuppressive role of adenosine as
323 mediated by WTAP. Finally, the level of IFN-γ in the PBMC culture supernatant was quantified 24
324 h after treatment using an IFN-γ detection ELISA kit (#KE00146, Proteintech, China) according to
325 the manufacturer's protocol.

326 **Subcutaneous xenograft experiments.** Twelve 4-week-old male nude mice were provided by
327 HuaFuKang Bioscience in Beijing. All mice were maintained under standard conditions in a sterile,
328 temperature-controlled environment (temperature 20 °C-26 °C and humidity approximately 50%) to
329 ensure the animals' comfort. After the mice had been allowed to adapt to local rearing conditions
330 for 1 week, 2×10^6 A375 cells were resuspended in 100 μl PBS and inoculated subcutaneously into
331 the left flank of the mice. After 1 week, following the formation of palpable punctate tumor masses
332 that were visible to the naked eye, the mice were randomly divided into two groups, and
333 cholesterol-modified siWTAP-2 or siNC (RiboBio, China) was injected intratumorally at a
334 concentration of 10 nmol/mouse once every week. The mice health and behavior were monitored
335 every day and the tumor volume and body weight of each mouse were recorded twice weekly, and
336 the tumor volume was calculated using the formula volume=length × width^2 × 0.5. The maximum
337 diameters of the tumors in each mouse did not exceed 2 cm. 7 days post the fourth inoculation (day
338 35 post tumor cell injection), all twelve mice survived the experiment and were subsequently
339 euthanized, and the tumors were completely removed for histological analysis. The detailed
340 procedure for the humane euthanasia of mice was as follows: First, anesthesia was induced by
341 placing the mouse under a face mask with 3-4% isoflurane in oxygen at a flow rate of 0.5-1 l/min
342 for 2-5 min until the corneal reflex was completely absent. Secondly, the isoflurane concentration
343 was set at 1.5-2% to ensure the maintenance of an anesthetic state and firm pressure was applied at
344 the base of the skull while gently pulling the tail to separate the cervical vertebrae from the skull.
345 Thirdly, death was confirmed by checking for the absence of reflexes again. The *in vivo*
346 experiments were approved by the Animal Care Committee of Shijiazhuang People's Hospital
347 (Approval No. 2024002).

348 **Statistical analysis.** SPSS software version 21.0 (IBM Corp.) and GraphPad Prism software 8.0

(Dotmatics) were used to analyzes the data and to generate the graphs, respectively. For measurement data, Student's t-test was used to compare two groups, while for datasets involving multiple group comparisons, one-way ANOVA (for parametric data) was adopted followed by LSD post hoc tests. Chi-square test was used to analyze clinical data. Patient prognosis was analyzed using the Kaplan-Meier method, and $p \leq 0.05$ and $p \leq 0.01$ were considered to indicate a statistically significant difference and highly statistically significant difference, respectively.

Results

WTAP acts as a cancer suppressor in melanoma. To explore WTAP expression in human melanoma tissues and its effect on melanoma malignancy, GEPIA dataset (https://gepia.cancer-pku.cn/) was adopted to examine the expression patterns of WTAP across various cancer types, and the analysis revealed that WTAP is significantly downregulated in Skin Cutaneous Melanoma (SKCM) compared to normal tissues (Figure 1A). Additionally, patients with low WTAP expression demonstrated a worse prognosis (Figure 1B).

To further validate our findings, we collected 55 human melanoma tissue samples and examined the expression of WTAP via IHC (Figure 1C). To further identify the correlation between the WTAP expression level and aggressive progression of melanoma, the 55 patients with melanoma were divided into two groups according to the median staining score: A group with low WTAP expression (n = 26) and another group with high WTAP expression (n=29). As shown in Table 2, WTAP expression was found to be negatively associated with the clinical stage and T classification of patients with melanoma, demonstrating that low WTAP expression is an aggressive characteristic of melanoma. Moreover, the clinical data analysis suggested that patients with lower WTAP expression had worse overall survival (OS) and disease-free survival (DFS) rates (Figures 1D, 1E). Furthermore, univariate analysis disclosed that WTAP expression, pathological T stage and clinical stage were significantly related to OS (Figure 1F), whereas multivariate analysis suggested that WTAP expression and pathological T stage were independent risk factors for OS (Figures 1G). Taken together, these findings confirmed that low WTAP expression is associated with a poor prognosis in patients with melanoma, demonstrating that WTAP may fulfil a suppressive role in melanoma progression.

WTAP suppresses melanoma cell proliferation, migration and invasion. To elucidate the

biological functions of WTAP in melanoma cells, three specific siRNAs directed against WTAP were used to knock down the expression of WTAP in A875 and A375 melanoma cells, and potential alterations in cell function were subsequently examined via a series of functional experiments. The knockdown efficiency of siRNAs targeting WTAP was first evaluated by RT-qPCR and western blotting analyses. As shown in Figure 2A and Supplementary Figure S1A, the results from both RT-qPCR and western blotting experiments revealed that siRNA-1 and siRNA-2 had greater knockdown efficiency compared with siRNA-3. Therefore, siRNA-1 and siRNA-2 were selected to downregulate endogenous WTAP expression in subsequent *in vitro* assays, and siRNA-2 was utilized to silence WTAP expression in RNA-seq and *in vivo* assays. The results of the CCK-8, EdU and colony formation assays demonstrated that a deficiency of WTAP led to substantial enhancement of the proliferative and clonogenic capabilities of A875 and A375 cells (Figures 2B, 2C; Supplementary Figure S2A). Furthermore, the results of the wound healing and Transwell assays revealed that WTAP downregulation clearly increased the migration and invasion of both cell types (Figures 2D, 2E). Moreover, to further examine the role of WTAP in melanoma cells, WTAP was overexpressed via a suitably designed plasmid, and the efficiency of transfection was confirmed via RT-qPCR and western blotting analyses (Figure 3A; Supplementary Figure S1B). WTAP was found to negatively influenced cell proliferation, as transfected A875 and A375 cells overexpressing WTAP exhibited decreased proliferative and clonogenic capabilities compared with those in the control group (Figures 3B, 3C; Supplementary Figure S2B). In addition, the forced overexpression of WTAP led to a markedly depletion of the migration and invasion rates of both cell types, as shown in Figures 3D and 3E. Taken together, these data highlighted that WTAP, which acts as a tumor suppressor protein, has a pivotal role in suppressing the proliferation, migratory and invasive capabilities of melanoma cells.

NT5E is the functional downstream target of WTAP in melanoma cells. To further explore the potential functional mechanism via which WTAP exerts a tumor suppressive effect in melanoma, transcriptome sequencing was employed to explore the transcriptional alterations in both siWTAP-2 A875 cells and parallel control siNC A875 cells. $|Log2FC| > 1$ and $p < 0.05$ were adopted as thresholds to identify altered genes following the deletion of WTAP in A875 cells, and six upregulated and eight downregulated genes were identified as potential downstream genes, as shown in volcano plots and heatmaps (Figures 4A, 4B). To further narrow the scope of downstream

targets, numerous previously published studies were consulted, and the genes Chromogranin B (CHGB), Inhibitor of nuclear factor kappa B kinase subunit gamma pseudogene 1 (IKBKGP1), NT5E, Solute carrier family 7 member 11 (SLC7A11), Fucosyltransferase 1 (FUT1) and Cystathionine gamma-lyase (CTH) were identified as potential targets involved in WTAP-mediated melanoma progression. RT-qPCR assays were subsequently performed to assess the impact of WTAP on each candidate gene. As shown in Figure 4C, NT5E was consistently found to be clearly upregulated upon transfecting both A875 and A375 cells with siWTAPs. Subsequently, immunofluorescence analysis was used to specifically identify the protein expression and subcellular localization of NT5E in siWTAP-transfected melanoma cells (Figure 4D). NT5E expression (shown by the green coloration) was clearly increased in both A875 and A375 cells following transfection with siWTAPs, as indicated by increased and brighter fluorescence levels located in the cell membrane and cytoplasm. Collectively, our findings identified NT5E as the key downstream effector of WTAP-mediated tumor suppression in melanoma.

Further analysis of the Kyoto Encyclopedia of Genes and Genomes (KEGG) pathway revealed that five differentially expressed genes were enriched in ten pathways (Figure 4E). The primary downstream gene NT5E was enriched in three pathways, namely, pyrimidine metabolism, nicotinate and nicotinamide metabolism, and Metabolic pathways. As demonstrated by previous studies, NT5E was able to hydrolyze AMP to produce extracellular adenosine, and this NT5E-adenosine pathway, has been reported both to extensively participate in cancer progression, metastasis and drug resistance, and to directly or indirectly affect pyrimidine metabolism, nicotinate and nicotinamide metabolism and metabolic pathways [37-39]. Based on the present evidences, we proposed that the NT5E-adenosine axis contributes to WTAP-dependent tumor regulation in melanoma. Therefore, to further confirm the activity of NT5E in melanoma cells, an AMPase hydrolysis assay was employed to evaluate NT5E function in melanoma cells following knockdown with siNC or siWTAPs. A875 or A375 cells were incubated with AMP, and the production of inorganic phosphate was assessed using the malachite green method. As shown in Figure 4F, in both A875 and A375 cells, WTAP knockdown led to a significant increase in inorganic phosphate production, which further confirmed that the elevated expression and function of NT5E in A875 and A375 cells was driven by transfection with the siWTAPs.

Inhibition of NT5E abrogated the effects of WTAP depletion in A875 and A375 cells. To further

439 determine whether the biological effect of WTAP on melanoma cells were mediated by NT5E, a
440 series of rescue experiments were performed. CCK-8 and colony formation assays revealed that the
441 deletion of NT5E led to a substantial reversal of the increases in the cell proliferative (Figure 5A)
442 and colony formation (Figure 5B) capabilities of both A875 and A375 cells caused by the silencing
443 of WTAP. Moreover, the depletion of NT5E also led to a marked suppression of the increased
444 migration and invasion rates of A875 and A375 cells that resulted from the attenuation of WTAP
445 (Figures 5C, 5D). Collectively, these data suggested that silencing WTAP effectively promoted the
446 malignant progression of melanoma cells through enhancing the activity of downstream NT5E.
447 **WTAP suppressed melanoma progression via NT5E-mediated immunosuppression and**
448 **molecular adhesion.** A growing body of evidence indicated that WTAP is widely involved in RNA
449 modifications associated with pre-mRNA splicing, miRNAs, lncRNAs, circRNA processing,
450 translation efficiency, and mRNA stability [40, 41]. Our present study also provides direct evidence
451 that WTAP depletion elevates NT5E transcript levels (Figures 4A-4C). In addition, to further
452 confirm whether WTAP could regulate NT5E mRNA, a RIP assay was implemented with A875 or
453 A375 cell lysates and either WTAP antibody or control rabbit IgG. As shown in Figure 6A, NT5E
454 mRNA was detected in the WTAP immunocomplexes, but not in the control IgG immunocomplexes,
455 and depletion of WTAP led to an increase in NT5E mRNA abundance in melanoma cell
456 supernatants. Actinomycin D chase experiments demonstrated that WTAP knockdown significantly
457 reduced the decay rate of NT5E mRNA in melanoma cells, indicating WTAP-mediated
458 destabilization of NT5E transcripts (Figure 6B).
459 A large body of evidence has shown that soluble NT5E, a major enzyme involved in the production
460 of extracellular adenosine via hydrolysing AMP, is able to suppress the function of T cells and to
461 fulfil an oncogenic role [42]. The expression of soluble NT5E has been confirmed to be higher in
462 patients with melanoma, demonstrating its potential as a predictive biomarker for immunotherapy
463 [43]. In this series of experiments, AMPase activity and IFN-γ production in the supernatant of the
464 melanoma cell cultures were examined to further evaluate NT5E activity. As shown in Fig. 6C,
465 compared with that of the siNC group, AMPase activity in the siWTAP group was clearly increased,
466 whereas the addition of NT5E inhibitor APCP to the supernatant impaired this NT5E-mediated
467 AMPase activity. As shown in Figure 6D, A875 and A375 cell culture supernatants were collected
468 and subsequently incubated with PBMCs, and PHA was added to the reaction mixtures to stimulate

469 the production of IFN-γ by PBMCs. PBMCs without PHA activation did not produce any
470 discernible level of IFN-γ; however, compared with that in activated cells without AMP, the
471 production of IFN-γ in PBMCs was substantially impaired when the substrate AMP was added to
472 the culture supernatant. Moreover, the addition of the NT5E inhibitor APCP partly reversed the
473 reduced secretion of IFN-γ compared with that in activated cells treated with AMP alone. As shown
474 in Figure 6E, the secretion of IFN-γ by PBMCs in the presence of AMP with or without the NT5E
475 inhibitor APCP was found to be depleted in the culture supernatant from siWTAP-treated A875 or
476 A375 cells. However, knocking down NT5E (siNT5E) rescued the decreased IFN-γ production
477 induced by both the siWTAP treated A875 and A375 cell supernatants, as shown in Figure 6F.
478 Overall, it was demonstrated that the increased expression of NT5E promoted by siWTAP in both
479 A875 and A375 cell cultures contributed to the hydrolysis of AMP to produce more adenosine,
480 which thereby subsequently abrogated the secretion of IFN-γ by PBMCs. Both the endogenic
481 deletion of NT5E by siNT5E treatment and exogenous inhibition of NT5E by APCP were shown to
482 suppress both its ability to produce adenosine and its immunosuppressive effect on PBMCs. To
483 further validate the role of the NT5E-adenosine pathway in WTAP-driven melanoma progression,
484 an A_{2A} adenosine receptor antagonist, AZD4635 was added to further ELISA assays. As shown in
485 Figure 6G, the addition of AZD4635 to the reaction enhanced secretion of IFN-γ compared to the
486 control experiments, suggesting that adenosine fulfils a critical role in NT5E-mediated IFN-γ
487 production, which further confirmed that NT5E-adenosine pathway contributed to WTAP-mediated
488 tumor suppression.
489 NT5E has an oncogenic role in tumor progression that is mediated via both enzymatic and
490 nonenzymatic activity [44]. In melanoma cells, the enzymatic function of NT5E is associated with
491 the cancer invasion process, whereas its nonenzymatic action is to increases cell migration and
492 ECM adhesion through the activation of focal adhesion kinase [44]. To further understand the
493 functional mechanism of NT5E in WTAP-mediated melanoma regression, the expression levels of
494 the Epithelial-Mesenchymal Transition (EMT)-associated markers Matrix Metalloproteinase 2
495 (MMP2) and N-cadherin in A875 and A375 cells were determined via western blotting. As shown
496 in Figures 7A and 7B, in WTAP-silenced melanoma cells, the expression level of NT5E, as well as
497 that of MMP2 and N-cadherin, was simultaneously increased. Moreover, NT5E deletion in
498 melanoma cells resulted in the downregulation of N-cadherin and MMP2 expression, whereas the

expression of WTAP was not significantly altered (Figures 7C, 7D). Furthermore, in the co-transfection assay, NT5E deficiency led to a reversal of the increase in MMP2 and N-cadherin expression induced by siWTAP in both A875 and A375 cells (Figures 7E, 7F).

WTAP suppressed melanoma tumorigenesis *in vivo*. To elucidate the role of WTAP in melanoma tumorigenesis *in vivo*, a xenograft melanoma tumorigenesis assay was performed by subcutaneously injecting A375 cells into nude mice (Figure 8A). The results obtained revealed that WTAP depletion promoted tumorigenesis, resulting in markedly larger tumor volumes and weights compared with the control mice (Figures 8B-8D). IHC analysis subsequently revealed that the xenograft tumors affected by siWTAP exhibited increased levels of NT5E, MMP2 and N-cadherin expression (Figure 8E). Taken together, these results suggested that WTAP exerts tumor-inhibiting effects on melanoma.

Discussion

Melanoma is the most malignant skin tumor with high invasive and metastatic potential, which is associated with poor outcomes [2]. Currently, cutaneous melanoma remains the leading cause of cutaneous cancer-associated deaths globally [3]. The multidisciplinary treatment of cutaneous melanoma is complicated, and therapeutic methods ranging from traditional surgery and chemotherapy to immunotherapy have gradually been developed in recent years [45]. m6A methylation is the predominant dynamic mRNA modification that occurs in all mammals [46], and aberrant m6A modifications have been ubiquitously identified in numerous types of cancers, including melanoma [47-49]. METTL3 drives aberrant uridine cytidine kinase 2 upregulation via m6A-dependent RNA stabilization, thereby activating the Wnt/β-catenin signaling axis to promote melanoma metastasis [47]. METTL14, while sharing functional synergy with METTL3 in m6A deposition, exhibits unique roles in modulating melanoma cell invasiveness through regulation of metastasis-associated transcripts [48]. Conversely, the m6A reader protein YTH N6-methyladenosine RNA binding protein 3 (YTHDF3) suppresses melanoma metastasis by binding m6A-modified lysyl oxidase-like 3 mRNA and destabilizing it, highlighting the context-dependent duality of m6A-mediated regulation in melanoma [49]. With respect to WTAP function in melanoma, Feng et al. [21] demonstrated an association between WTAP expression and prognosis in patients with melanoma through analyzing databases, and further performed functional

assays in which A375 cells were used to overexpress WTAP. However, the underlying mechanism via which WTAP suppresses melanoma progression has yet to be fully elucidated.

In the present study, both the expression and mechanism of action of WTAP in the development of melanoma were carefully investigated. WTAP was found to be downregulated in melanoma tissues, and WTAP expression was significantly negatively correlated with clinical stage and T stage, according to the IHC analysis of melanoma tissues. In addition, WTAP expression, pathological T stage and clinical stage were strongly related to OS, and WTAP expression and pathological T stage were found to be independent risk factors for OS. Subsequently, the role of WTAP in the proliferation and invasion of melanoma cells was explored. A series of functional assays revealed that an attenuation of WTAP expression led to substantial increases in cell proliferation and invasion, whereas WTAP overexpression led to a decrease in the proliferation and invasion of melanoma cells. Furthermore, data obtained from *in vivo* animal experiments confirmed the tumor suppressor function of WTAP in melanoma cells, as melanoma xenografts generated with siWTAP cells formed larger tumors in nude mice compared with the tumors generated with control cells. Subsequently, NT5E was identified as a potential downstream target via RNA-seq analysis, and an ectonucleotidase assay and ELISA were then performed with the aim of verifying NT5E expression and function in cells with silenced WTAP expression. The rescue and western blot assays that were performed demonstrated that silencing NT5E abrogated the upregulated effects and EMT-associated gene expression caused by WTAP depletion in melanoma cells. Mechanistically speaking, RIP and Actinomycin D experiments demonstrated that WTAP binds to the mRNA of the downstream gene NT5E and destabilizes it, thereby suppressing melanoma progression. Collectively, these data suggested that WTAP suppresses melanoma progression via NT5E-regulated EMT and adenosine pathway.

By contrast, abundant evidence has shown that WTAP contributes to aggressive features in other malignant tumors, where it serves as a considerable risk factor [14-17]. For example, WTAP is highly expressed in hepatocellular carcinoma, and is associated with poor survival. Functionally, WTAP increases the proliferation and growth of hepatocellular carcinoma cells, and the overexpression of WTAP was found to promote the progression of hepatocellular carcinoma through reducing the expression of the downstream suppressor gene ETS proto-oncogene 1 [14]. In addition, WTAP is highly upregulated in osteosarcoma tissue, and as an oncogene, WTAP was

559 shown to facilitate the proliferation and metastasis of osteosarcoma cells by regulating the stability
560 of the downstream suppressor gene homeobox containing 1 [15]. WTAP is a conserved nuclear
561 protein that functions as a partner of Wilms' tumor 1 (WT1) [50], which was previously identified
562 as an inactivated tumor suppressor gene in a subset of pediatric renal cancers [51]. Additionally,
563 WT1 has been described as a tumor suppressor in various kinds of cancer [52, 53]. With regard to
564 WTAP as a tumor suppressor gene, as shown in Figure 1A, the GEPIA dataset revealed that WTAP
565 is significantly downregulated in several cancer types, including SKCM, Thyroid carcinoma, Breast
566 invasive carcinoma, Kidney Chromophobe, Lung adenocarcinoma. Through a systematic literature
567 review, we identified only three robust bioinformatics studies supporting the tumor-suppressive role
568 of WTAP [18-20]. However, no experimental studies have explicitly validated its tumor-suppressive
569 function, and the precise molecular mechanisms underlying this activity remain unclear due to the
570 absence of detailed mechanistic investigations. In our present study, a RIP assay was implemented
571 with A875 or A375 cell lysates and WTAP antibody, and NT5E mRNA was detected in the WTAP
572 immunocomplexes, and depletion of WTAP led to an increase in NT5E mRNA abundance in
573 melanoma cell supernatants. Further Actinomycin D chase experiments demonstrated that WTAP
574 knockdown significantly reduced the decay rate of NT5E mRNA in melanoma cells, all of which
575 suggested that WTAP was able to bind to NT5E mRNA and exerts tumor-suppressive effects in
576 melanoma by modulating NT5E mRNA stability. Each tumor therefore evolves in its own unique
577 way, and in the case of melanoma, WTAP may exhibit behavior as a tumor suppressor gene,
578 fulfilling a suppressive role in melanoma progression.
579 Systemic management of melanoma has been revolutionized by the development of targeted
580 therapies and immunotherapies. Immune checkpoint inhibitor therapy has sparked new hope for
581 therapies against melanoma, especially advanced melanoma. In the present study, WTAP was
582 shown to play a tumor suppressor role in melanoma *in vitro* and *in vivo*. Through transcriptome
583 sequencing, the downstream target gene NT5E was identified as a potential factor. As a
584 well-studied gene, NT5E has been shown to be overexpressed in numerous types of cancer, and its
585 high expression both contributes to tumor malignancy and is associated with poor outcomes [27-29].
586 In recent years, a growing body of data have shown that NT5E is considered an ideal therapeutic
587 target for cancer therapy, especially in situations where conventional therapy and/or treatment are
588 combined with other immune checkpoint inhibitors, since its hydrolysis produces the

589 immunosuppressive compound adenosine, which further increases tumor growth and metastasis [22,
590 23]. Therefore, NT5E depletion, in general, is expected to expedite the immune response to limit
591 tumor-mediated immune evasion, especially in advanced melanoma. In the present study, either
592 blocking NT5E by adding APCP to the melanoma culture supernatant or inhibiting NT5E
593 expression via siRNAs led to a marked reduction in adenosine production, thereby improving
594 adenosine-mediated IFN-γ secretion. The addition of an A_{2A} adenosine receptor antagonist,
595 AZD4635 to the reaction enhanced secretion of IFN-γ compared to the control experiments,
596 suggesting that adenosine fulfils a critical role in NT5E-mediated IFN-γ production, which further
597 confirmed that NT5E-adenosine pathway contributed to WTAP-mediated tumor suppression. These
598 results provided further evidence in support of NT5E, downstream from WTAP, having an
599 immunosuppressive role in melanoma progression, and these findings were consistent with the
600 previously demonstrated immunosuppressive function of NT5E. Additionally, NT5E effects
601 molecular adhesion to promote malignant tumor progression. The results from the western blot
602 analysis experiments revealed that the expression levels of MMP2 and N-cadherin were upregulated
603 in the siWTAP groups, and that reduced NT5E expression led to a reversal of the elevated levels of
604 MMP2 and N-cadherin expression that resulted from WTAP silencing in both A875 and A375 cells.
605 Collectively, these findings have provided sufficient evidence to enable us to conclude that novel
606 interventions to increase WTAP expression may have the effect of attenuating the NT5E-mediated
607 immunosuppressive role, which would thereby exert an influence on molecular adhesion to
608 suppress melanoma progression.
609 In conclusion, the present study has clearly demonstrated that WTAP is downregulated in
610 melanoma, which impedes the progression of melanoma via the downstream effects mediated by
611 NT5E on immunosuppression and molecular adhesion. The present study has also determined that
612 WTAP exerts a crucial inhibitory role in melanoma oncogenesis, thereby highlighting WTAP as a
613 potentially novel diagnosis and therapeutic target in melanoma.
614
615 Acknowledgements: The present study was supported by funding from the Natural Science
616 Foundation of Hebei Provence (No. H2022206368) and the Cultivating Programme Plan for
617 Clinical Excellent Talent of Hebei in 2024 (No. ZF2024067).
618

Supplementary data are available in the online version of the paper.

References

[1] SWETTER SM, JOHNSON D, ALBERTINI MR, BARKER CA, BATENI S et al. NCCN Guidelines® Insights: Melanoma: Cutaneous, Version 2.2024. J Natl Compr Canc Netw 2024; 22: 290-298. https://doi.org/10.6004/jnccn.2024.0036

[2] GARBE C, AMARAL T, PERIS K, HAUSCHILD A, ARENBERGER P et al. European consensus-based interdisciplinary guideline for melanoma. Part 1: Diagnostics: Update 2022. Eur J Cancer 2022; 170: 236-255. https://doi.org/10.1016/j.ejca.2022.03.008

[3] REBECCA VW, SOMASUNDARAM R, HERLYN M. Pre-clinical modeling of cutaneous melanoma. Nat Commun 2020; 11: 2858. https://doi.org/10.1038/s41467-020-15546-9

[4] FADADU RP, WEI ML. Ultraviolet A radiation exposure and melanoma: a review. Melanoma Res 2022; 32: 405-410. https://doi.org/10.1097/CMR.0000000000000857

[5] MILLER KD, NOGUEIRA L, DEVASIA T, MARIOTTO AB, YABROFF KR et al. Cancer treatment and survivorship statistics, 2022. CA Cancer J Clin 2022; 72: 409-436. https://doi.org/10.3322/caac.21731

[6] WEI G. RNA m6A modification, signals for degradation or stabilisation? Biochem Soc Trans 2024; 52: 707-717. https://doi.org/10.1042/BST20230574

[7] HUANG S, WYLDER AC, PAN T. Simultaneous nanopore profiling of mRNA m6A and pseudouridine reveals translation coordination. Nat Biotechnol 2024; 42: 1831-1835. https://doi.org/10.1038/s41587-024-02135-0

[8] LIU Z, GAO L, CHENG L, LV G, SUN B et al. The roles of N6-methyladenosine and its target regulatory noncoding RNAs in tumors: classification, mechanisms, and potential therapeutic implications. Exp Mol Med 2023; 55: 487-501. https://doi.org/10.1038/s12276-023-00944-y

[9] ZACCARA S, RIES RJ, JAFFREY SR. Reading, writing and erasing mRNA methylation. Nat Rev Mol Cell Biol 2019; 20: 608-624. https://doi.org/10.1038/s41580-019-0168-5

[10] ZHAO J, LU L. Interplay between RNA Methylation Eraser FTO and Writer METTL3 in Renal Clear Cell Carcinoma Patient Survival. Recent Pat Anticancer Drug Discov 2021; 16: 363-376. https://doi.org/10.2174/1574892816666210204125155

[11] HAUSSMANN IU, BODI Z, SANCHEZ-MORAN E, MONGAN NP, ARCHER N et al. m6A potentiates Sxl alternative pre-mRNA splicing for robust Drosophila sex determination. Nature 2016; 540: 301-304. https://doi.org/10.1038/nature20577

[12] MOINDROT B, CERASE A, COKER H, MASUI O, GRIJZENHOUT A et al. A Pooled shRNA Screen Identifies Rbm15, Spen, and Wtap as Factors Required for Xist RNA-Mediated Silencing. Cell Rep 2015; 12: 562-572. https://doi.org/10.1016/j.celrep.2015.06.053

[13] HUME S, DIANOV GL, RAMADAN K. A unified model for the G1/S cell cycle transition. Nucleic Acids Res 2020; 48: 12483-12501. https://doi.org/10.1093/nar/gkaa1002

[14] CHEN Y, PENG C, CHEN J, CHEN D, YANG B et al. WTAP facilitates progression of hepatocellular carcinoma via m6A-HuR-dependent epigenetic silencing of ETS1. Mol Cancer 2019; 18: 127. https://doi.org/10.1186/s12943-019-1053-8

[15] CHEN S, LI Y, ZHI S, DING Z, WANG W et al. WTAP promotes osteosarcoma tumorigenesis by repressing HMBOX1 expression in an m6A-dependent manner. Cell Death Dis 2020; 11: 659. https://doi.org/10.1038/s41419-020-02847-6

[16] WANG J, ZHENG F, WANG D, YANG Q. Regulation of ULK1 by WTAP/IGF2BP3 axis enhances mitophagy and progression in epithelial ovarian cancer. Cell Death Dis 2024; 15: 97. https://doi.org/10.1038/s41419-024-06477-0

[17] TAN YT, LI T, WANG RB, LIU ZK, MA MY et al. WTAP weakens oxaliplatin chemosensitivity of colorectal cancer by preventing PANoptosis. Cancer Lett 2024; 604: 217254. https://doi.org/10.1016/j.canlet.2024.217254

[18] LEI J, FAN Y, YAN C, JIAMALIDING Y, TANG Y et al. Comprehensive analysis about prognostic and immunological role of WTAP in pan-cancer. Front Genet 2022; 13: 1007696. https://doi.org/10.3389/fgene.2022.1007696

[19] SHI J, XIE G, YE S, WENG X, ZHOU Q. Pan-cancer analysis reveal that m6A writer WTAP involve in tumor cell cycle regulation and tumor immunity. Discov Oncol 2025; 16: 426. https://doi.org/10.1007/s12672-025-02196-w

[20] FU Y, SUN S, BI J, KONG C, YIN L. Expression patterns and prognostic value of m6A RNA methylation regulators in adrenocortical carcinoma. Medicine (Baltimore) 2021; 100: e25031. https://doi.org/10.1097/MD.0000000000025031

[21] FENG ZY, WANG T, SU X, GUO S. Identification of the m6A RNA Methylation Regulators WTAP as a Novel Prognostic Biomarker and Genomic Alterations in Cutaneous Melanoma. Front Mol Biosci 2021; 8: 665222. https://doi.org/10.3389/fmolb.2021.665222

[22] CHIARELLA AM, RYU YK, MANJI GA, RUSTGI AK. Extracellular ATP and Adenosine in Cancer Pathogenesis and Treatment. Trends Cancer 2021; 7: 731-750. https://doi.org/10.1016/j.trecan.2021.04.008

[23] XU JG, CHEN S, HE Y, ZHU X, WANG Y et al. An antibody cocktail targeting two different CD73 epitopes enhances enzyme inhibition and tumor control. Nat Commun 2024; 15: 10872. https://doi.org/10.1038/s41467-024-55207-9

[24] LIU W, YU X, YUAN Y, FENG Y, WU C et al. CD73, a Promising Therapeutic Target of Diclofenac, Promotes Metastasis of Pancreatic Cancer through a Nucleotidase Independent Mechanism. Adv Sci (Weinh) 2023; 10: e2206335. https://doi.org/10.1002/advs.202206335

[25] PETRUK N, TUOMINEN S, AKERFELT M, MATTSSON J, SANDHOLM J et al. CD73 facilitates EMT progression and promotes lung metastases in triple-negative breast cancer. Sci Rep 2021; 11: 6035. https://doi.org/10.1038/s41598-021-85379-z

[26] LUPIA M, ANGIOLINI F, BERTALOT G, FREDDI S, SACHSENMEIER KF et al. CD73 Regulates Stemness and Epithelial-Mesenchymal Transition in Ovarian Cancer-Initiating Cells. Stem Cell Reports 2018; 10: 1412-1425. https://doi.org/10.1016/j.stemcr.2018.02.009

[27] ZHU J, DU W, ZENG Y, LIU T, LI J et al. CD73 promotes non-small cell lung cancer metastasis by regulating Axl signaling independent of GAS6. Proc Natl Acad Sci U S A 2024; 121: e2404709121. https://doi.org/10.1073/pnas.2404709121

[28] PETRUK N, WOOD SL, GREGORY W, LOPEZ-GUAJARDO A, OLIVA M et al. Increased primary breast tumor expression of CD73 is associated with development of bone metastases and is a potential biomarker for adjuvant bisphosphonate use. Sci Rep 2025; 15: 9449. https://doi.org/10.1038/s41598-025-92841-9

[29] CHATTERJEE A, CHAUDHARY A, GHOSH A, ARUN P, MUKHERJEE G et al. Overexpression of CD73 is associated with recurrence and poor prognosis of gingivobuccal

oral cancer as revealed by transcriptome and deep immune profiling of paired tumor and margin tissues. Cancer Med 2023; 12: 16774-16787. https://doi.org/10.1002/cam4.6299

[30] DELGIORNO K. CD73 Is a Critical Immune Checkpoint in a Molecular Subtype of Pancreatic Cancer. Cancer Res 2023; 83: 977-978. https://doi.org/10.1158/0008-5472.CAN-23-0268

[31] XIA C, YIN S, TO KKW, FU L. CD39/CD73/A2AR pathway and cancer immunotherapy. Mol Cancer 2023; 22: 44. https://doi.org/10.1186/s12943-023-01733-x

[32] GOSWAMI S, WALLE T, CORNISH AE, BASU S, ANANDHAN S et al. Immune profiling of human tumors identifies CD73 as a combinatorial target in glioblastoma. Nat Med 2020; 26: 39-46. https://doi.org/10.1038/s41591-019-0694-x

[33] LIAN W, JIANG D, LIN W, JIANG M, ZHANG Y et al. Dual role of CD73 as a signaling molecule and adenosine-generating enzyme in colorectal cancer progression and immune evasion. Int J Biol Sci 2024; 20: 137-151. https://doi.org/10.7150/ijbs.87440

[34] HOEK KS, EICHHOFF OM, SCHLEGEL NC, DOBBELING U, KOBERT N et al. In vivo switching of human melanoma cells between proliferative and invasive states. Cancer Res 2008; 68: 650-656. https://doi.org/10.1158/0008-5472.CAN-07-2491

[35] SCHMITTGEN TD, LIVAK KJ. Analyzing real-time PCR data by the comparative C(T) method. Nat Protoc 2008; 3: 1101-1108. https://doi.org/10.1038/nprot.2008.73

[36] WINK MR, LENZ G, BRAGANHOL E, TAMAJUSUKU AS, SCHWARTSMANN G et al. Altered extracellular ATP, ADP and AMP catabolism in glioma cell lines. Cancer Lett 2003; 198: 211-218. https://doi.org/10.1016/s0304-3835(03)00308-2

[37] SCALETTI E, HUSCHMANN FU, MUELLER U, WEISS MS, STRATER N. Substrate binding modes of purine and pyrimidine nucleotides to human ecto-5'-nucleotidase (CD73) and inhibition by their bisphosphonic acid derivatives. Purinergic Signal 2021; 17: 693-704. https://doi.org/10.1007/s11302-021-09802-w

[38] JAMES EL, LANE JA, MICHALEK RD, KAROLY ED, PARKINSON EK. Replicatively senescent human fibroblasts reveal a distinct intracellular metabolic profile with alterations in NAD+ and nicotinamide metabolism. Sci Rep 2016; 6: 38489. https://doi.org/10.1038/srep38489

[39] DENG Y, CHEN Q, YANG X, SUN Y, ZHANG B et al. Tumor cell senescence-induced macrophage CD73 expression is a critical metabolic immune checkpoint in the aging tumor microenvironment. Theranostics 2024; 14: 1224-1240. https://doi.org/10.7150/thno.91119

[40] LI ZX, ZHENG ZQ, YANG PY, LIN L, ZHOU GQ et al. WTAP-mediated m(6)A modification of lncRNA DIAPH1-AS1 enhances its stability to facilitate nasopharyngeal carcinoma growth and metastasis. Cell Death Differ 2022; 29: 1137-1151. https://doi.org/10.1038/s41418-021-00905-w

[41] REN Z, HU Y, SUN J, KANG Y, LI G et al. N6-methyladenosine methyltransferase WTAP-stabilized FOXD2-AS1 promotes the osteosarcoma progression through m(6)A/FOXM1 axis. Bioengineered 2022; 13: 7963-7973. https://doi.org/10.1080/21655979.2021.2008218

[42] WANG M, JIA J, CUI Y, PENG Y, JIANG Y. CD73-positive extracellular vesicles promote glioblastoma immunosuppression by inhibiting T-cell clonal expansion. Cell Death Dis 2021; 12: 1065. https://doi.org/10.1038/s41419-021-04359-3

[43] TURIELLO R, CAPONE M, MORRETTA E, MONTI MC, MADONNA G et al. Exosomal CD73 from serum of patients with melanoma suppresses lymphocyte functions and is

associated with therapy resistance to anti-PD-1 agents. J Immunother Cancer 2022; 10: e004043. https://doi.org/10.1136/jitc-2021-004043

[44] SADEJ R, SKLADANOWSKI AC. Dual, enzymatic and non-enzymatic, function of ecto-5'-nucleotidase (eN, CD73) in migration and invasion of A375 melanoma cells. Acta Biochim Pol 2012; 59: 647-652.

[45] NENCLARES P, AP DAFYDD D, BAGWAN I, BEGG D, KERAWALA C et al. Head and neck mucosal melanoma: The United Kingdom national guidelines. Eur J Cancer 2020; 138: 11-18. https://doi.org/10.1016/j.ejca.2020.07.017

[46] TANG J, ZHOU C, YE F, ZUO S, ZHOU M et al. RNA methylation homeostasis in ocular diseases: All eyes on Me. Prog Retin Eye Res 2025; 105: 101335. https://doi.org/10.1016/j.preteyeres.2025.101335

[47] WU H, XU H, JIA D, LI T, XIA L. METTL3-induced UCK2 m6A hypermethylation promotes melanoma cancer cell metastasis via the WNT/β-catenin pathway. Ann Transl Med 2021; 9: 1155. https://doi.org/10.21037/atm-21-2906

[48] ZHUANG A, GU X, GE T, WANG S, GE S et al. Targeting histone deacetylase suppresses tumor growth through eliciting METTL14-modified m6 A RNA methylation in ocular melanoma. Cancer Commun (Lond) 2023; 43: 1185-1206. https://doi.org/10.1002/cac2.12471

[49] SHI HZ, XIONG JS, GAN L, ZHANG Y, ZHANG CC et al. N6-methyladenosine reader YTHDF3 regulates melanoma metastasis via its 'executor'LOXL3. Clin Transl Med 2022; 12: e1075. https://doi.org/10.1002/ctm2.1075

[50] LITTLE NA, HASTIE ND, DAVIES RC. Identification of WTAP, a novel Wilms' tumour 1-associating protein. Hum Mol Genet 2000; 9: 2231-2239. https://doi.org/org/10.1093/oxfordjournals.hmg.a018914

[51] TORBAN E, GOODYER P. Wilms' tumor gene 1: lessons from the interface between kidney development and cancer. Am J Physiol Renal Physiol 2024; 326: F3-F19. https://doi.org/10.1152/ajprenal.00248.2023

[52] MZIK M, CHMELAROVA M, JOHN S, LACO J, SLABY O et al. Aberrant methylation of tumour suppressor genes WT1, GATA5 and PAX5 in hepatocellular carcinoma. Clin Chem Lab Med 2016; 54: 1971-1980. https://doi.org/10.1515/cclm-2015-1198

[53] YAO Y, CHAI X, GONG C, ZOU L. WT1 inhibits AML cell proliferation in a p53-dependent manner. Cell Cycle 2021; 20: 1552-1560. https://doi.org/10.1080/15384101.2021.1951938

Figure Legends

Figure 1. WTAP expression was downregulated in melanoma. A) The expression levels of WTAP mRNA across various cancers were analyzed by GEPIA datasets. B) Kaplan-Meier survival curves for OS in melanoma patients were generated using data from GEPIA datasets. C) The protein expression of WTAP in melanoma tissues was analyzed by IHC (n=55) (magnification, ×200). D, E) Kaplan-Meier survival curves of OS and DFS in melanoma patients were constructed based on WTAP immunohistochemical staining. The log-rank test was used to compare differences between

two groups. F, G) Forest plots were constructed based on the outcomes of univariate and multivariate analyses of several factors associated with the OS and RFS of melanoma patients. *p < 0.05, **p < 0.01

Figure 2. Deletion of WTAP enhanced the growth and invasion of melanoma cells. A) Negative control or siRNA (siWTAP-1, siWTAP-2 and siWTAP-3) was transfected into A875 and A375 cells, and the knockdown efficiency was determined by RT-qPCR. B, C) Melanoma cell proliferation was detected via CCK-8 and EdU assays (magnification, ×200). D, E) Scratch healing and Transwell assays were applied to compare melanoma cell migration and invasion (magnification, ×100). **p < 0.01

Figure 3. WTAP overexpression weakened the growth and invasion of melanoma cells. A) The plasmid for WTAP overexpression and control vector were transfected into A875 and A375 cells, and the efficiency of infection was determined by RT-qPCR. B, C) The proliferation of melanoma cells was detected by CCK-8 and EdU assays (magnification, ×200). D, E) The migration and invasion of melanoma cells were evaluated via a scratch healing and Transwell assays (magnification, ×100). *p < 0.05, **p < 0.01

Figure 4. NT5E was proven to be a downstream target of WTAP in melanoma progression. A, B) Volcano plots and heatmaps were generated from the differentially expressed genes identified via RNA-seq. C) Relative mRNA expression levels of representative genes in A875 and A375 cells treated with siWTAP-2. D) Immunofluorescence staining of NT5E in A875 and A375 cells transfected with siWTAP (magnification, ×200). E) Enrichment analysis for representative KEGG pathways in WTAP target genes. F) AMPase activity of A875 and A375 cell culture supernatants in the siWTAP and siNC groups. **p < 0.01

Figure 5. siNT5E reversed the effects of siWTAP on increasing the proliferation and metastasis of melanoma cells. A, B) Compared with the siNC+siNC group, the siNC+siNT5E group presented suppressed proliferation and colony formation in melanoma cells, and compared with the siWTAP+siNC group, the siWTAP+siNT5E group presented impaired proliferation and colony

formation in melanoma cells. C, D) The migration and invasion of melanoma cells were lower in the siNC+siNT5E group than in the siNC+siNC group, and the migration and invasion of melanoma cells were lower in the siWTAP+siNT5E group than in the siWTAP+siNT5E group (magnification, ×100). *$p < 0.05$, **$p < 0.01$

Figure 6. NT5E-mediated immunosuppression is involved in WTAP-dependent suppression of melanoma progression. A) A875 and A375 cell lysates were supplemented with anti-WTAP and anti-IgG antibodies to determine whether WTAP interacts with NT5E mRNA. B) Actinomycin D assay was adopted to examine NT5E stability changes in WTAP-knockdown melanoma cells. C) AMPase activity was determined in the supernatants of siWTAP- and siNC-transfected melanoma cell cultures. AMP was used as a substrate, APCP was used as an inhibitor, and the amount of released inorganic phosphate was measured via the Malachite Green assay. D) ELISA was used to measure IFN-γ levels in the supernatants of PBMC cultures with or without the PHA activator and melanoma cell cultures with or without the NT5E substrate AMP and the selective NT5E inhibitor APCP. E) IFN-γ levels in the supernatant of PHA-activated PBMCs cultured with supernatant from siWTAP or siNC melanoma cells in the presence of AMP with or without APCP were measured via ELISA. F) ELISA was performed to detect IFN-γ levels in the supernatant of PHA-activated PBMC cultures treated with culture supernatant of melanoma cells transfected with both siWTAP and siNT5E by the addition of AMP and APCP in every reaction. G) The secretion of IFN-γ was detected via ELISA in each reaction with or without AZD4635. *$p < 0.05$, **$p < 0.01$

Figure 7. WTAP expression was assessed in melanoma cells transfected with siWTAP, siNT5E, or both. A-D) The protein expression of WTAP, NT5E, MMP2 and N-cadherin in the siWTAP and siNT5E groups compared with that in the siNC group was assessed via western blotting. E, F) The protein expression of WTAP, NT5E, MMP2 and N-cadherin in A875 and A375 cells was observed after transfection with siWTAP, siNT5E and both siWTAP and siNT5E. **$p < 0.01$

Figure 8. WTAP inhibited melanoma cell growth *in vivo*. A) Schematic diagram of the groups in the xenotransplantation model. B) Images of xenografts in the indicated groups. C, D) Volume (C) and weight (D) of subcutaneous xenograft tumors. E) Representative immunohistochemical images

854 of WTAP, NT5E, MMP2 and N-cadherin in xenograft tumors from the siWTAP-2 and siNC groups
855 (magnification, ×200). **$p < 0.01$
856

857 **Table 1.** Primer sequences and reaction conditions.

Gene	Primer sequence	Annealing temperature	Product size, bp
WTAP	F: 5' -TTCCCAAGAAGGTTCGATTG-3' R: 5' -TGCAGACTCCTGCTGTTGTT-3'	57 °C	192
CHGB	F: 5' -TCTATCCCTCCGACAGCCAA-3' R: 5' -CGTCGTTTGTCCACCTCAGA-3'	59 °C	412
IKBKGP1	F: 5' -GCACCTCTCCAGCCTCCATC-3' R: 5' -CGCTTTTGTGTACCTTTGTGTATCTC-3'	57 °C	113
NT5E	F: 5' -CTCCTCTCAATCATGCCGCT-3' R: 5' -TGGATTCCATTGTTGCGTTCA-3'	59 °C	174
SLC7A11	F: 5' -TGGAACGAGGAGGTGGAGAA-3' R: 5' -TGGTGGACACAACAGGCTTT-3'	57 °C	264
FUT1	F: 5' -CCCCTGCATCCCCGATCT-3' R: 5' -GGTCTGGACACAGGATCGAC-3'	57 °C	195
CTH	F: 5' -CTCACTGTCCACCACGTTCA-3' R: 5' -CTGTTTGTACAGTACTTAGCCCC-3'	55 °C	138
GAPDH	F: 5' -AATCCCATCACCATCTTCCA-3' R: 5' -TGGACTCCACGACGTACTCA-3'	57 °C	82

858 Abbreviations: WTAP-Wilms' tumor 1-associating protein; NT5E-ecto-5'-ucleotidase;
859 CHGB-Chromogranin B; IKBKGP1-Inhibitor of Kappa Light Polypeptide Gene Enhancer in
860 B-cells, Kinase Gamma Pseudogene 1; SLC7A11-Solute Carrier Family 7 Member 11;
861 FUT1-Fucosyltransferase 1; CTH-Cystathionine Gamma-Lyase;
862 GAPDH-Glyceraldehyde-3-Phosphate Dehydrogenase
863

Table 2. Clinicopathological features of melanoma patients.

Characteristics	Level	Low	High	χ2	p-value
n		26	29		
Age (years)	< 60	11	16	0.908	0.341
	≥ 60	15	13		
Sex	Male	16	13	1.536	0.215
	Female	10	16		
Stage	I	2	6	9.193	0.027
	I	6	14		
	I	10	7		
	I	8	2		
T classification	T2	8	19	6.827	0.033
	T3	11	7		
	T4	7	3		
N classification	N0	11	19	5.053	0.168
	N1	5	6		
	N2	7	2		
	N3	3	2		
M classification	M0	11	16	0.908	0.341
	M1	15	13		

Note: a chi-square test was used to compare groups with low and high WTAP expression; *$p < 0.05$

Fig. 1 Download full resolution image

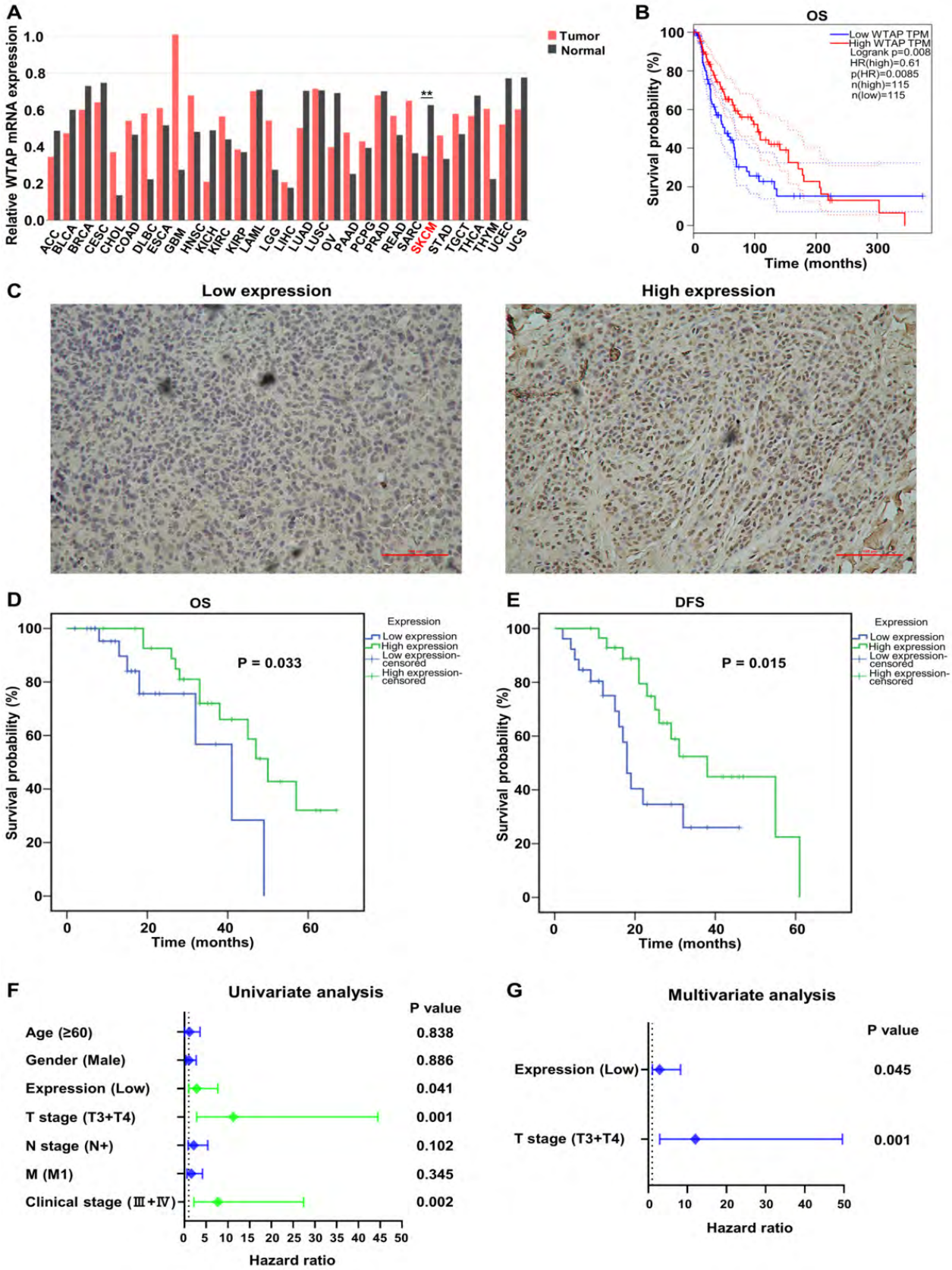

Fig. 2 Download full resolution image

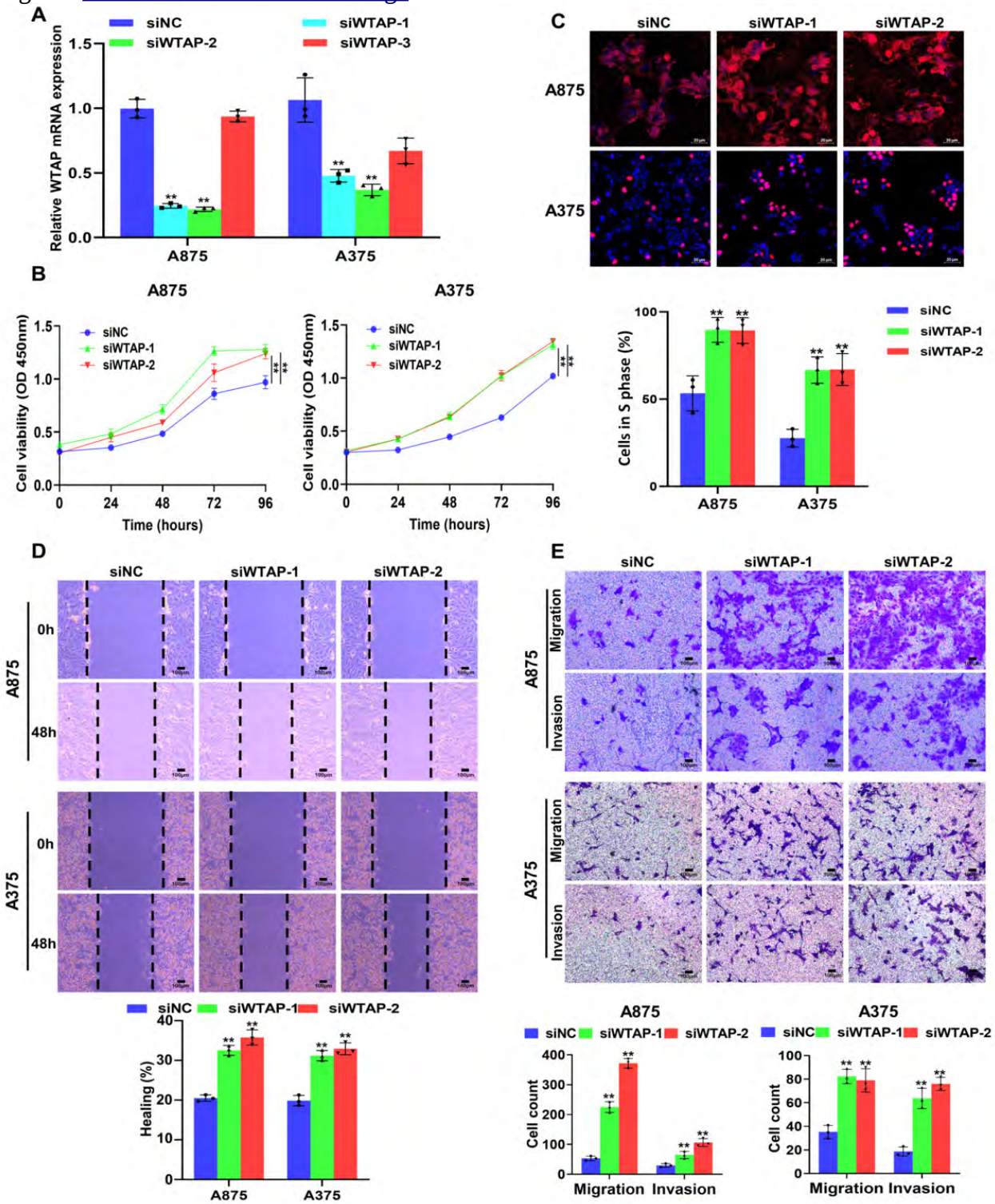

Fig. 3 Download full resolution image

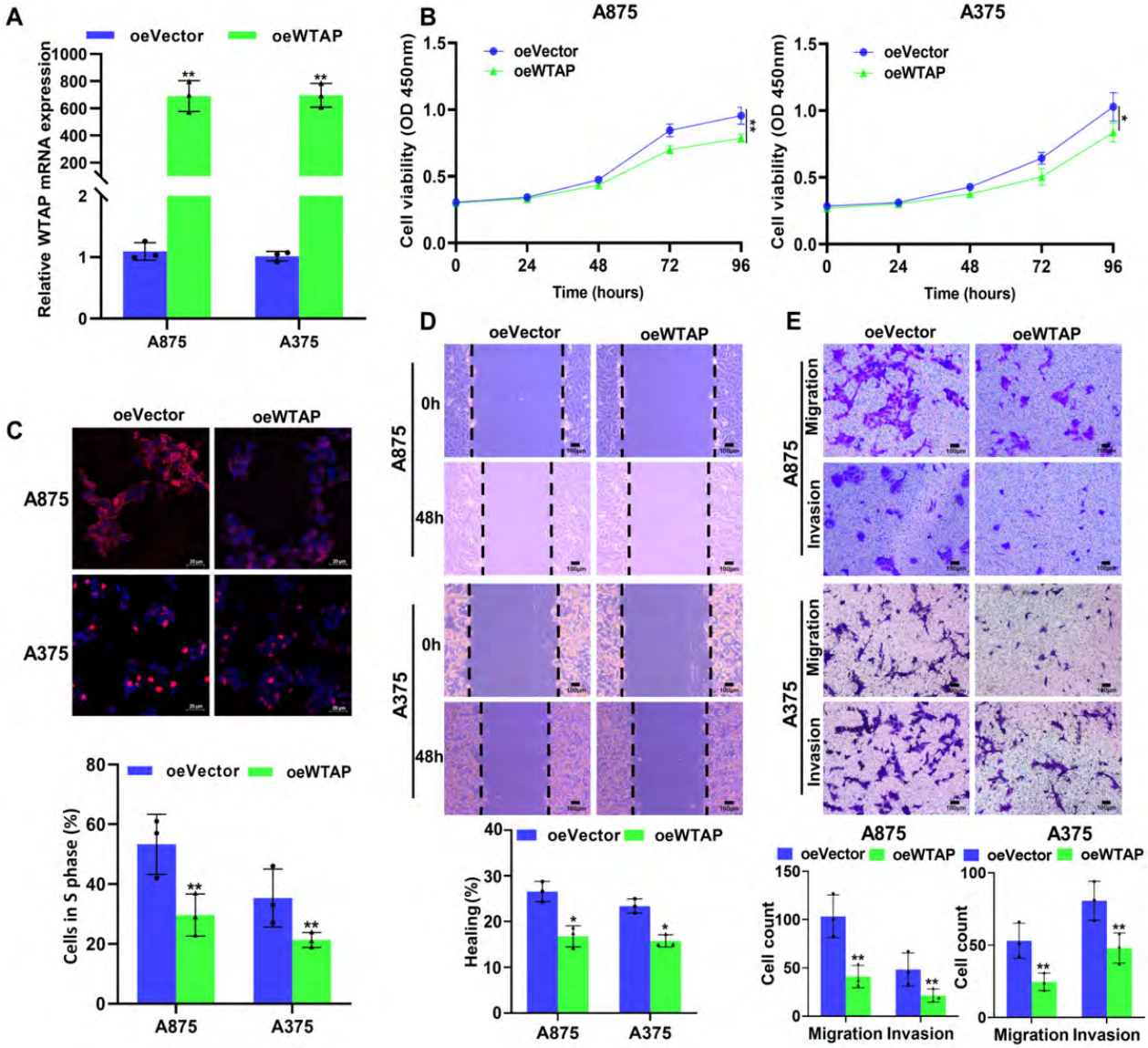

Fig. 4 [Download full resolution image]

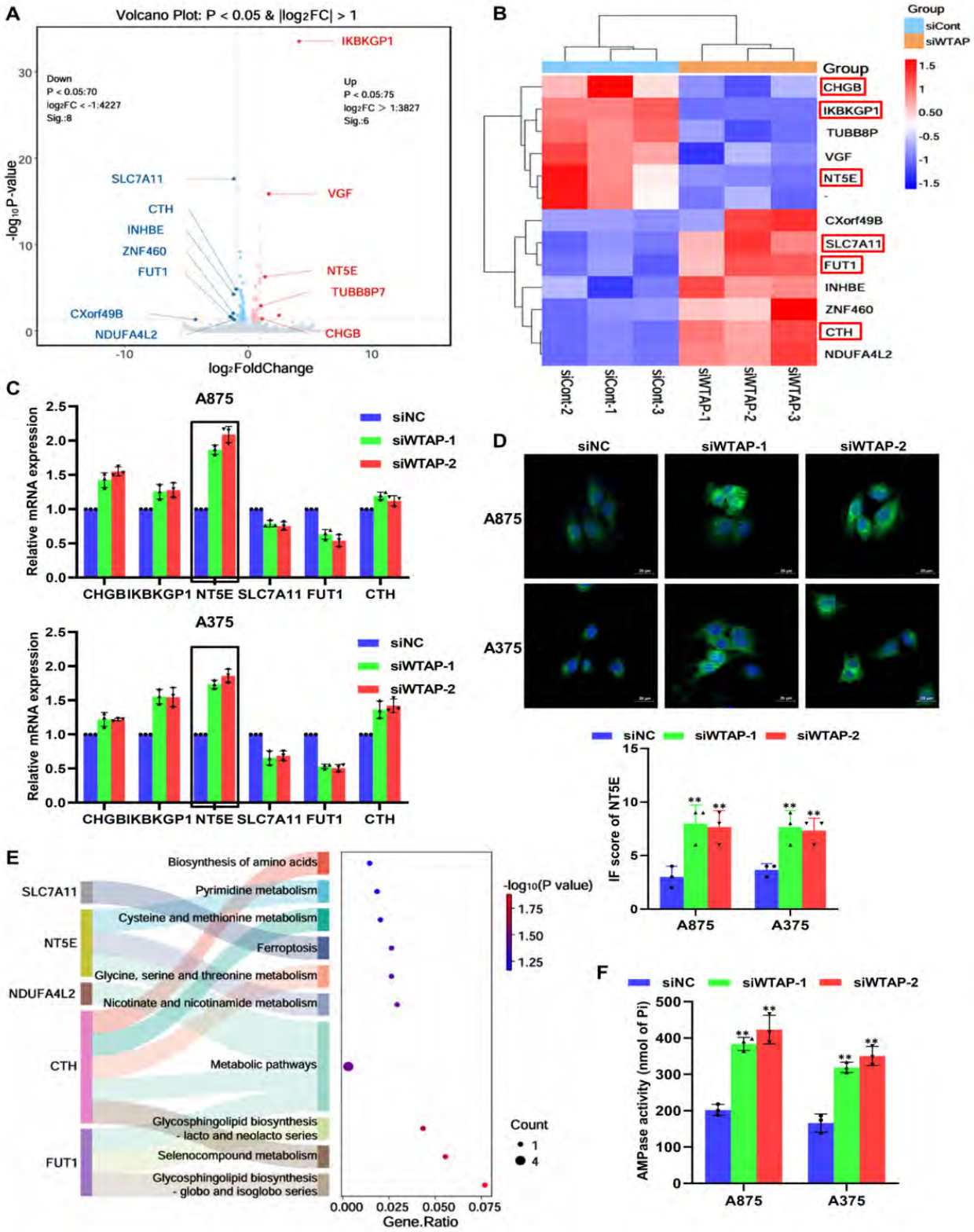

Fig. 5 Download full resolution image

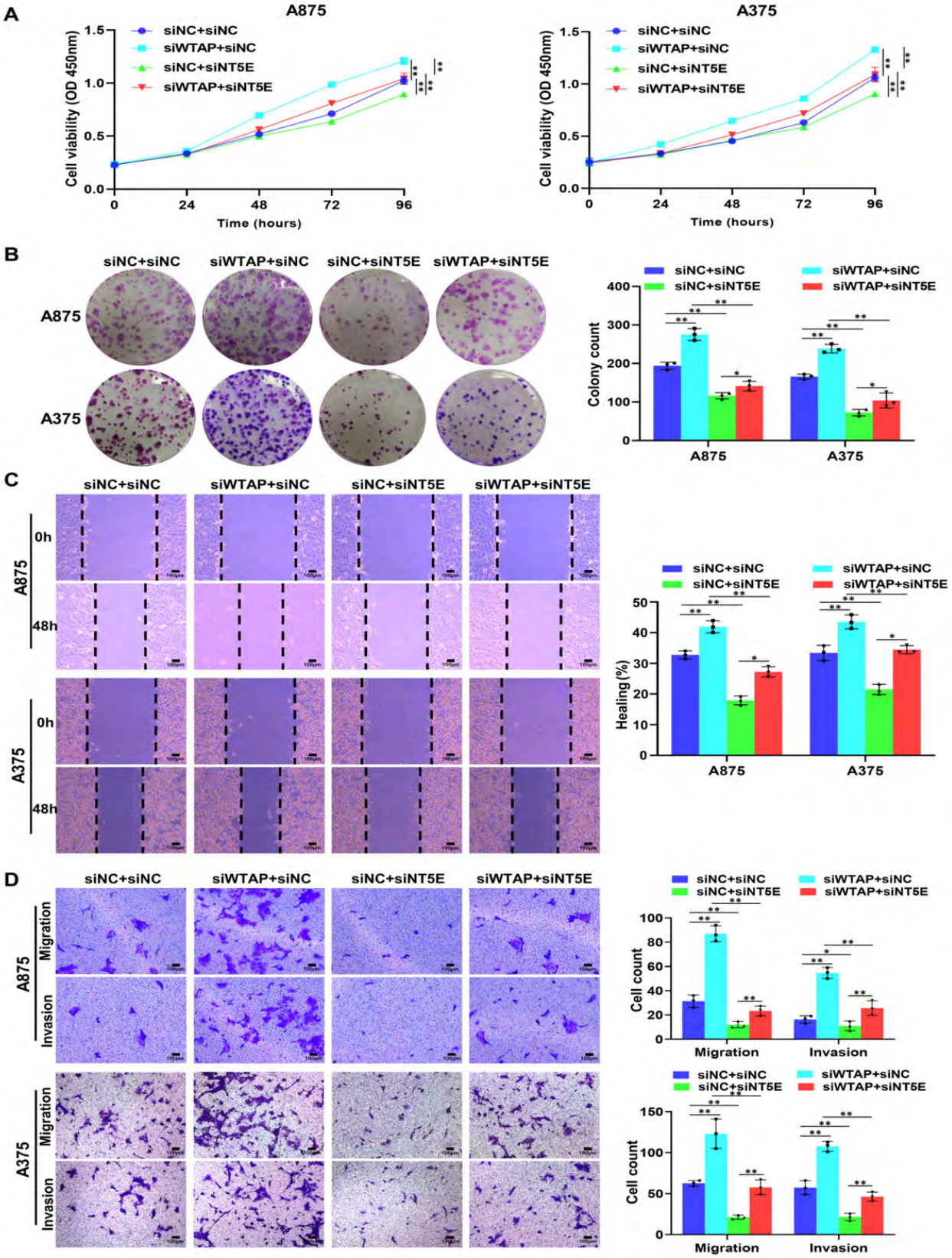

Fig. 6 Download full resolution image

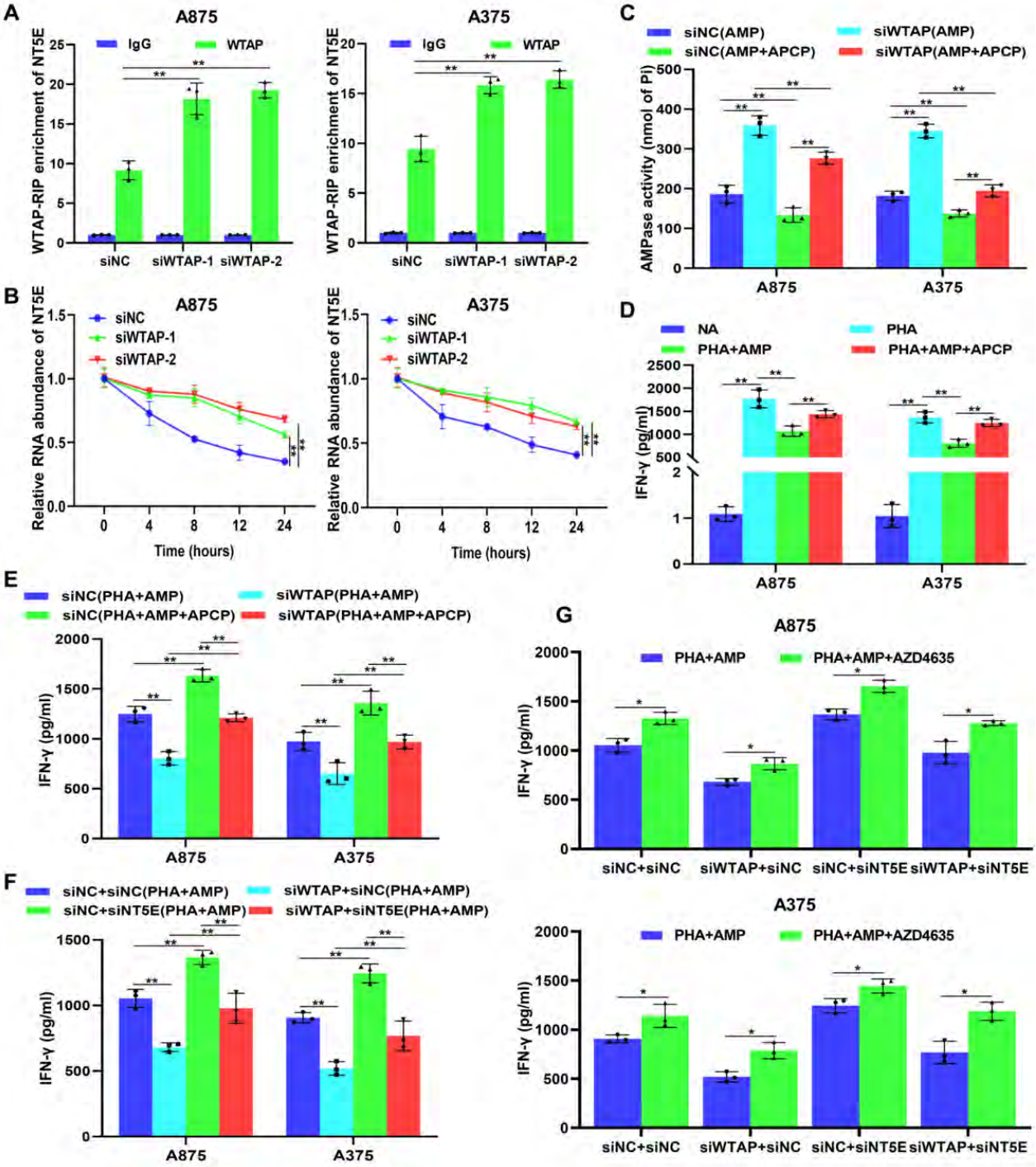

Fig. 7 Download full resolution image

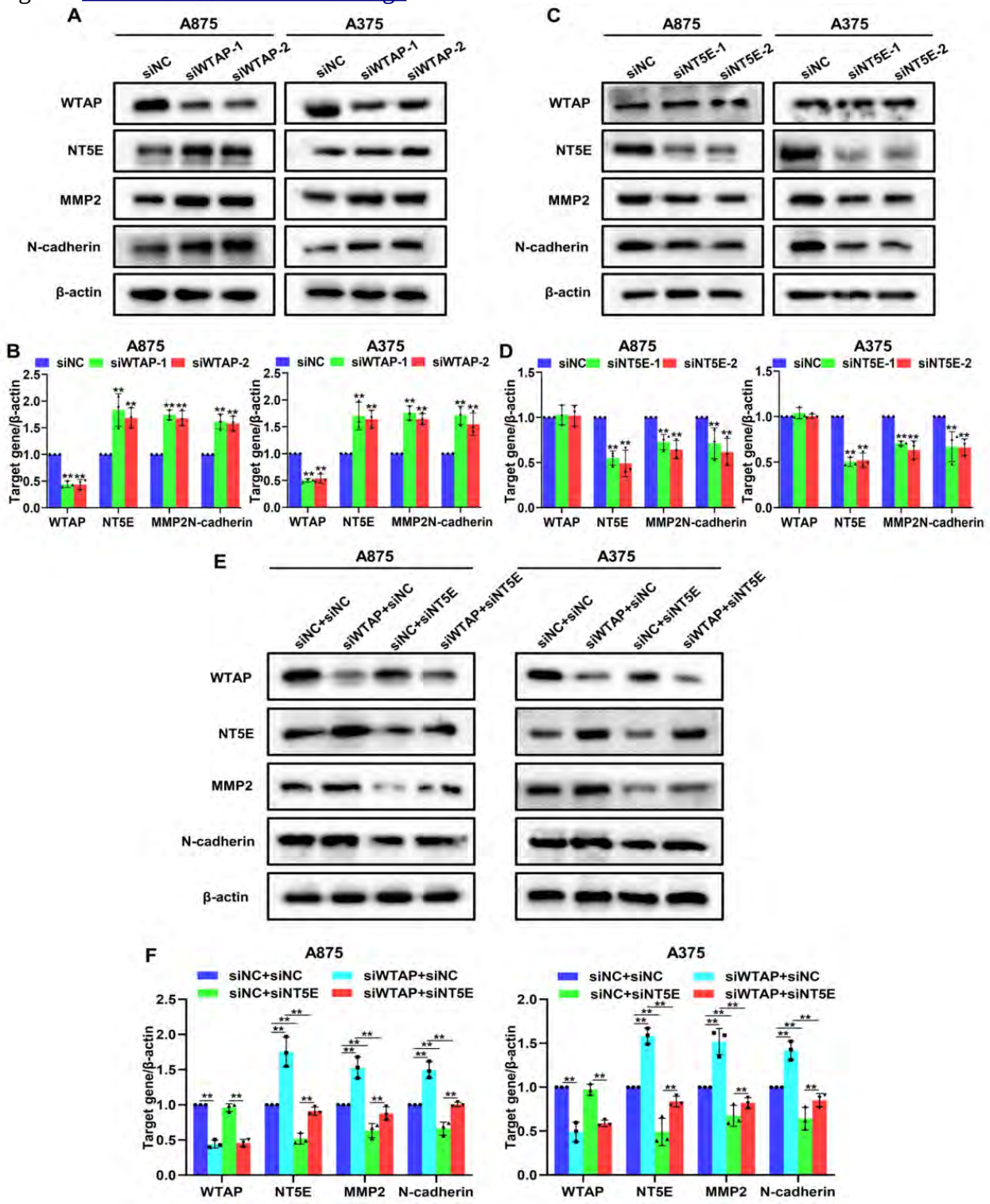

Fig. 8 Download full resolution image